Hard axes magnetic specific heat measurements in rare-earth copper compounds

Nives Bonacic
Department of Physics, Faculty of Science, University of Zagreb, Bijenicka 32, 10000 Zagreb

Supervisor: Prof. Dr. Christian Pfleiderer
SCES (E-51), Department of Physics, TU Munich, James-Franck-Str. 1, 85748 Garching

Abstract

The implementation of an experimental set-up for temperature and field-dependent measurements of heat capacity in materials with strong electronic correlations and large magnetic anisotropies is presented. To ensue the mechanical stability against torques acting on the sample when applying magnetic fields along the hard axes, an Al plate sample platform was designed to fit the Heat capacity option of the Physical Property Measurements System (PPMS). Specific heat was measured in the cubic rare-earth (RE) copper compounds HoCu and ErCu along the $\langle 110 \rangle$ axis in fields up to 14T .

1 Introduction

Measuring heat capacity provides key information on phase transitions, revealing the nature of excitations and changes of entropy across phase boundaries. In magnetic materials with complex phase diagrams, strong mechanical torque renders measurements in finite magnetic fields futile with present-day experimental apparatus. In order to remedy this limitation, the sample was fixed to a stable sample stage. Data gathering and evaluation were optimised for magnetic phase transitions in materials of interest.

1.1 Motivation

The project was inspired by the recent discoveries of topologically non-trivial magnetic phases such as skyrmion lattice, which was experimentally verified in 2009 [1]. In particular, the materials concerned are rare-earth intermetallics with possibly complex spin textures such as HoCu, ErCu and TmCu. Two common ways of determining whether a material has a non-trivial topological order are Hall-effect measurements and neutron scattering. One precondition for such a magnetic phase to arise is the existence of multi-k magnetic orderings which were reported by Morin et al. [2] for the three materials chosen in this study.

The RE-Cu compounds crystallise in the CsCl-type structure and are chemically almost identical, since their 4f shells lie shielded beneath Xe orbitals. Therefore, the variation of physical properties reflects mainly the character of the 4f state, principally its magnetic moment.

RE-Cu displayed a large topological Hall-effect signals on the order of $\mu\Omega$cm which is one order of magnitude larger than the largest topological contribution in the A-phase of MnSi, indicating a complex spin structure [3]. Neutron scattering observed antiferromagnetic ordering in this sub-class of rare earth intermetallics. Their high symmetry narrows down the number of possible structures dramatically. Relying on the crystal field anisotropy insights, the magnetic moments are likely directed in $\langle 100 \rangle$, $\langle 110 \rangle$ or $\langle 111 \rangle$ directions.

1.2 Previous studies

Measurements of the specific heat of cubic RE-Cu were performed on polycrystalline samples in zero magnetic field by Morin et al. [4]. Though their investigations were limited to polycrystalline materials, they showed multi-step magnetism, intricate magnetic phase diagrams, complex magnetic structures and quadrupolar order in selected compounds.

Single crystals were prepared in our group using optical float zoning and magnetic phase diagrams were obtained for all three compounds (HoCu [5], ErCu [6]). Both of these studies performed feature tracking of magnetisation and ac-susceptibility, partially resistivity and Hall-effect, and attempted heat capacity measurements in field, but results have eluded so far. ErCu was chosen for this study and its magnetic phase diagram is given in Figure 1 in $\langle 110 \rangle$, resulting from magnetisation, ac-susceptibility and heat capacity. Three magnetic phases exist in zero-field and a number of possible phases may be induced by the magnetic field.

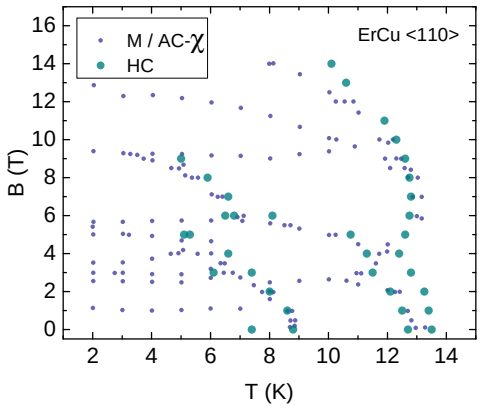

Figure 1: Phase diagram of ErCu for the ⟨110⟩ crystallographic direction as determined from magnetisation, ac-susceptibility and measurements of heat capacity

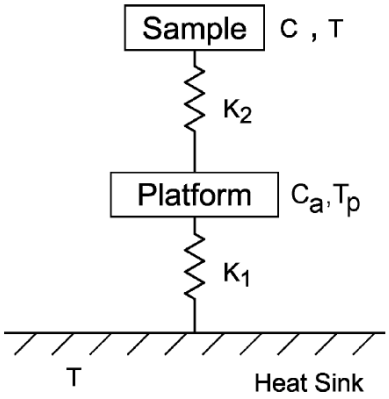

Figure 2: Heat flow diagram for a standard calorimeter using thermal relaxation calorimetry

2 Thermal relaxation calorimetry

The Physical Property Measurements System (PPMS) enables performing various experiments with precise thermal control such as magnetometry, electrical transport, thermal transport or adapting the basic platform for unique configurations [7]. The available sample environment includes magnetic fields up to ±14T and a $(1.8-400)$K temperature range. PPMS Multi Vu software application is used for executing measurements and collecting data.

2.1 Deriving the model

The Heat capacity option measures heat capacity at constant pressure $C_p = (\mathrm{d}Q/\mathrm{d}T)_p$ by a relaxation technique. The heat flow diagram for a standard calorimeter is depicted in Figure 2. A sample of unknown heat capacity C is attached to a sample platform with adhesive. The platform thermometer and heater are attached to the bottom of the platform. Combined addenda heat capacity of the platform, thermometer, heater and adhesive, amounts to C_a.

Heat is added with power $P(t)$ for a fixed time at the sample platform with changing temperature T_p, after which a relaxation period τ_1 to the thermal bath at stable T_b occurs. Temperature response is recorded during the heating and the cooling process.

The time constant of the relaxation period depends on total heat capacity $C_{tot} = C + C_a$, and thermal conductance K_1 between the platform and the thermal bath. Thermal conductance of the adhesive K_2 should provide a fast response τ_2 ($\tau_2 \ll \tau_1$) in the sample temperature T. Heat-balance condition for the system is described with the following equations [8]

$$\begin{aligned} P &= C_a \frac{\mathrm{d}T_p}{\mathrm{d}t} + K_2(T_p - T) + K_1(T_p - T_b) \\ 0 &= C\frac{\mathrm{d}T}{\mathrm{d}t} + K_2(T - T_p) \end{aligned} \tag{1}$$

Assuming an ideal thermal contact between the sample and the platform, the heat balance equation simplifies to

$$P = (C_a + C)\frac{\mathrm{d}T_p}{\mathrm{d}t} + K_1(T_p - T_b) \tag{2}$$

When the heat flowing to the platform is discontinued, the sample platform temperature follows the simple expression

$$T_p = T_b + \Delta T \exp\left(-t/\tau\right) \tag{3}$$

with a time constant $\tau = (C + C_a)/K_1$. Disregarding the time dependence of C, C_a and K_1 for a small ΔT ($\Delta T \ll T$), Eq (3) determines C from a measured τ. Addenda heat capacity is measured with no sample attached to the platform and K_1 is determined from measuring ΔT. Data analysis automatically subtracts the addenda heat capacity from the calibration and fits the model, yielding a value of heat capacity C.

If the thermal contact of the adhesive is not sufficient to secure $K_2 \gg K_1$, the thermal decay involves the sum of two exponentials such as in Figure 3

$$T_p(t) = T + A\exp\left(-t/\tau_1\right) + B\exp\left(-t/\tau_2\right) \tag{4}$$

2.2 Data analysis

Measured decay curves can be fitted with the Hwang-model [9] to obtain τ_1, τ_2, K_2 and C, for known values of C_a and K_1. The sample temperature is logged as a function of time, each pulse consisting of 256 data

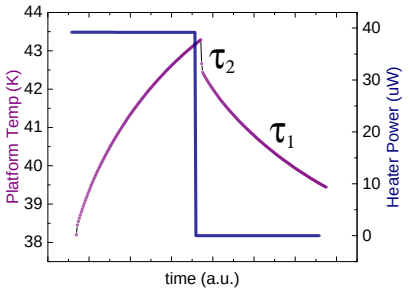

Figure 3: Typical heater and platform temperature time dependence in PPMS for a pulse with two-tau decay

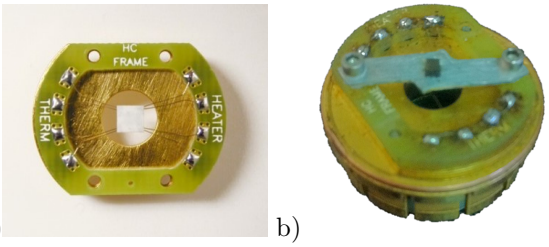

a) b)

Figure 4: a) Conventional puck frame for measuring heat capacity in PPMS
b) Al plate setup for measuring heat capacity of magnetically complex systems in fields mounted on the HC frame and assembled to a PPMS puck

points. It is common to distinguish the small heat pulse method from the quasi-adiabatic large pulse method. An analysis of the PPMS performance and limitations was carried out by Lashley and al. [10].

Small pulse technique employs a heat pulse resulting in ΔT of about $0.1\% - 2\%$ of the current sample temperature. Many small pulses are applied at different temperatures which can be time consuming if τ_1 is overly large. In addition, this approach [11] neglects variations of sample specific heat over the temperature range of a single pulse. This is not necessarily true near a first-order phase transition.

In the large pulse technique, typical pulse size is 30% and the heating and cooling curve are treated individually using the following equation [12]

$$C_{tot}\left(T\right) = \frac{-K_2(T - T_b) + P(T)}{\mathrm{d}T/\mathrm{d}t} \tag{5}$$

Usually, a moving average of up to 10% is applied in the post-processing, which reduces the scattering of data points and causes a smearing of sharp anomalies. To account for switching the heater on and off, it is possible to exclude the initial part of the pulse. A considerable overlap in temperature is required for neighbouring pulses. For fast scans, especially at higher temperatures, heat capacity is derived using the dual-slope method [13]. Heating and cooling curves are combined by interpolation, assuming a symmetric pulse as follows

$$C_{tot} = \frac{P_h\left(T\right) - P_c\left(T\right)}{\left.\frac{\mathrm{d}T}{\mathrm{d}t}\right|_h + \left.\frac{\mathrm{d}T}{\mathrm{d}t}\right|_c} \tag{6}$$

2.3 Conventional PPMS setup

The conventional setup for the PPMS heat capacity option consists of a sapphire or Al_2O_3 platform of $3 \times 3\mathrm{mm}^2$, suspended on eight 75μm Au-Pd wires such as in Figure 4 a). They provide mechanical support, thermal path K_1 and electrical contact for the sample platform. The sample is mounted using a thin layer of Apiezon N grease, which serves as the thermal contact to the platform K_2. The thermal connection to the thermal bath is dominated by the conductance of the wiring $K_1 \sim 6\mathrm{mW/K}$ (at 15K) since the sample space can be evacuated to high-vacuum. This gives a reproducible heat link with corresponding time constant sufficient to allow both sample platform and sample to achieve thermal equilibrium in the range of seconds.

Problems were encountered when measuring heat capacity in large magnetic fields along different crystallographic axes. In magnetic fields along the hard axis, there exists a torque on the sample which leads to its detaching from the sample platform or tilting of the platform. Since the sample is only weakly fixed to the measurement platform by vacuum grease, it will easily turn towards a more favourable orientation. Moreover, the direction of the hard axis can change at a specific field and temperature, making the results ambiguous.

2.4 Bespoke Al plate setup

The challenge was keeping the sample fixed by increasing mechanical support, while keeping the heat capacity measurable. When adding parts to the original setup, it is necessary to calculate their effect on the time constants and to adjust their material, size and shape so that the relation between them remains similar. I have introduced a new design, calculated the relevant parameters (C_a, K_1, τ_1) and experimentally established an appropriate measuring routine for the available samples. This design, shown in Figure 4 b), consists of an aluminium plate (0.5mm) instead of the sample platform, which dominantly determines the addenda heat capacity, and fiberglass spacers, which define the thermal conductivity.

Aluminium was selected among the nonmagnetic machinable materials because of its low density. It consequently gives an overall smaller heat capacity than

the heat capacity of other materials with similar specific heat. Since it is a good thermal and electrical conductor it needs to be separated from the bath to permit gradual relaxation.

Fiberglass spacers were chosen for this purpose, because of their low heat capacity and thermal conductance. Precise defining and tuning of the thermal link is achieved by the geometry of the spacers, the area of contact with the heat sink and their thickness (0.5mm) .

A Cernox temperature sensor CX-1010 is used as a thermometer and a Ruthenium Oxide 1kΩ temperature sensor is used as a heater. Small bare chips were added manually, fixed with GE varnish and contacted with four 30μm manganine wires using silver epoxy. Manganine has significantly lower thermal conductance than the conventional Au-Pd wiring. It is thus assumed that the thermal contact is given solely through the fiberglass spacers.

The sample is attached by Stycast 2850 FT, a two component, thermally conductive epoxy. It gives a strong permanent connection of the sample to the sample platform. Its addenda contribution is comparable with the addenda of the Apiezon N grease in the conventional setup.

Characteristic properties of the two setups at 15K are given in Table 1. Both addenda heat capacity and the conductance of the Al setup are scaled by a factor of 100, leaving their ratio unchanged. The sample heat capacitiy is usually $(2-10)$ mJ/K, still enabling good resolution using the PPMS automatic data acqusition. All additional heat capacities are negligible in comparison to the heat capacity of the Al plate. Test measurements of the platform heat capacity were in accordance with the calibration data for the temperature range of interest, assuring that the platform achieves thermal equilibrium, despite its heat capacity being much larger than the heat capacity of the conventional setup.

at 15K	K_1	C_a	$\tau_a = C_a/K_1$
conventional	6mW/K	35μJ/K	$\sim$ 6ms
Al plate	0.1W/K	0.5mJ/K	$\sim$ 5ms

Table 1: Characteristic properties of the conventional setup and the Al plate setup at 15K

The new setup produces reliable information for investigated RE-Cu compounds in the temperature range where anomalies occur. For higher temperatures than 50K, the sample heat capacity of these materials is much smaller than the addenda heat capacity and comparable with the error of the addenda heat capacity, thus the conventional setup must be used. Lower temperature measurements below 2K, would necessitate adjusting the mechanical, thermal and electrical path separately, such as in the Kevlar setup, currently under development.

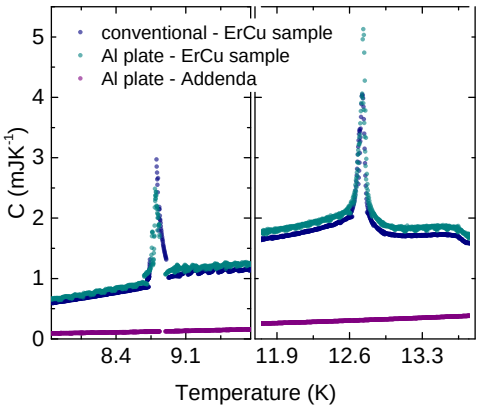

Figure 5: Comparison of ErCu heat capacity for the conventional and Al plate setups in the temperature range of interest, small pulse 2%, dual-slope processing, moving average 5%, exclusion 5%

3 Results

The studied materials are anisotropic, show numerous anomalies and exhibit magnetic torque when measured along the hard axis, leading to loss of the sample from the sample platform or its tilting towards the new easy axis. With the new Al plate setup, the sample is fixed with a strong adhesive on a mechanically stable platform, which solves this issue and enables access to specific heat values in magnetic fields. Data obtained by the conventional and the Al plate setup for ErCu in zero field are presented in Figure 5, showing good agreement. Heat capacity of the Al setup itself is significantly smaller than the sample heat capacity in this temperature range.

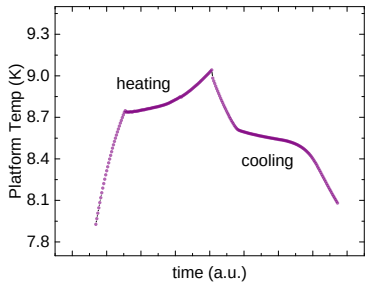

Figure 6: An asymmetrical pulse at the first order phase transition in ErCu

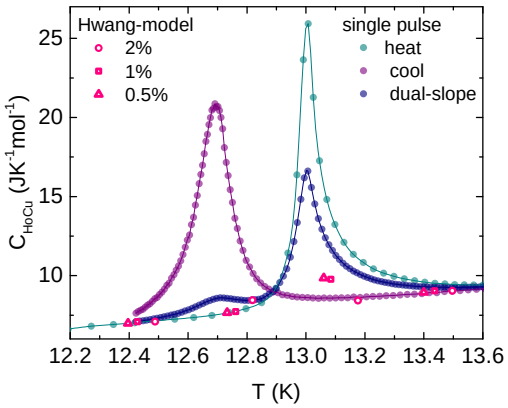

Figure 7: Post-processing procedures of large pulse method for HoCu sample in the vicinity of a phase transition

3.1 Fitting routines

Large overall heat capacity can lead to a nonsymmetrical pulse (Figure 6) due to the heat drag from the sample and the sample platform. As a result, the heating and cooling curve disagree on the position and size of the phase transition, especially around first order phase transitions, involving latent heat.

The heating process is faster than the cooling process, resulting in less data points, but its position agrees with the small pulse technique which is not susceptible to this ambiguity (Figure 7).

Using the dual-slope method, a larger peak is observed at the correct phase transition temperature of the heating curve with a better statistics, almost equivalent to the cooling curve. The drawback of this method is a potential smaller second peak on the phase transition temperature of the cooling curve, owing to the aforementioned asymmetry. Nevertheless, this method is preferred for data analysis.

3.2 Pulse size

Larger pulses cover the temperature range with shorter measurement time, however may give erroneous data when multiple phase transitions are encountered during a single pulse. Since the number of data points is fixed for any pulse size and duration, a larger pulse results in lower density of points. On the other hand, the pulse size should not be smaller than the size of the phase transition itself and smaller pulses require more points, i.e. longer measurement times.

Specific heat of HoCu at a phase transition is presented in Figure 8 for different large pulse sizes, restricting the maximal pulse size. It is required that the heating curve consist of more than ten data points for measurements to be regarded as relevant. For studied RE-Cu materials, the transitions are in the temperature range $(7-30)$K and some are as narrow as 0.2K, setting the appropriate pulse size to $(10-20)\%$.

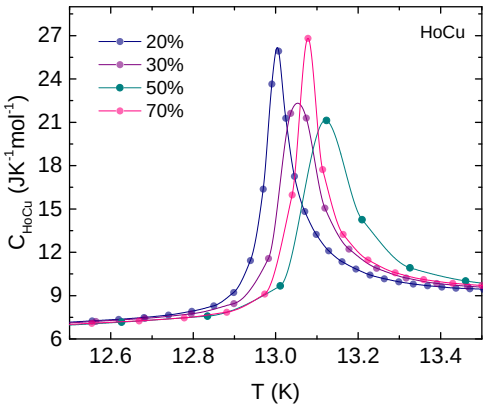

Figure 8: Specific heat of HoCu at a phase transition from heating curve for pulse sizes (20-70)% , moving average 10%, exclusion 10%

3.3 Magnetic phase diagram of ErCu

An ErCu sample $(1.75\times1.5\times1)\,\mathrm{mm}^3$ was attached to the new sample platform and its specific heat was measured along the $\langle110\rangle$ axis in fields up to 14T. The results are shown in Figure 9, separated by 5Jmol^{-1}K^{-1} with increasing field. They were obtained with a 20% pulse $(2-50)\,\mathrm{K}$, using the dual-slope post-processing with 10% moving average and 10% initial exclusion.

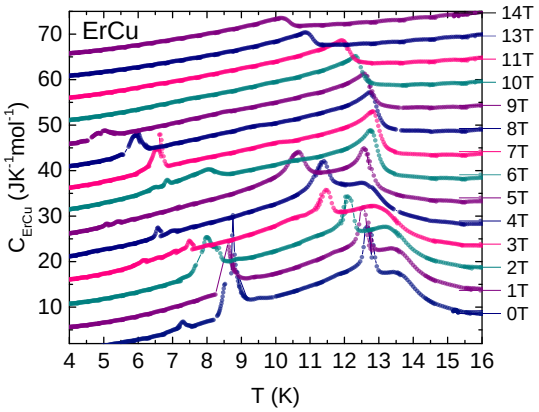

Figure 9: Specific heat of ErCu in magnetic field along the $\langle110\rangle$ axis, pulse size 20%, moving average 10%, exclusion 10%. For clarity the data are shifted by an offset of 5Jmol^{-1}K^{-1} with increasing field

ErCu sample was chosen as the smallest of presently available samples, since the heat capacity of these compounds is unusually large at low temperatures causing long time constants (~ 100s). This compound is the most challenging for analysis of the three compounds since the phase transitions are on a lower temperature scale than those in HoCu, however closer and wider than the phase transitions in TmCu, which has the lowest phase transition temperatures.

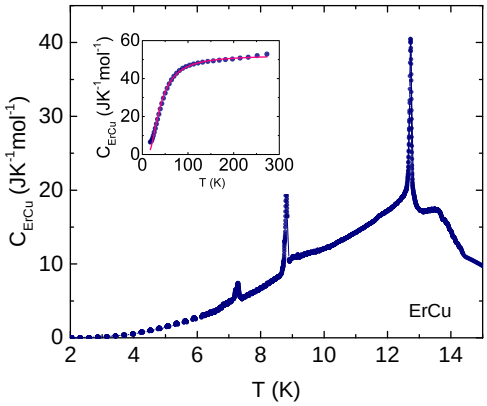

Figure 10: Specific heat of ErCu in zero field, pulse size 20%, moving average 10%, exclusion 10%, inset showing the Einstein model fit for higher temperatures using the conventional setup with a small pulse of 2%

Zero field measurements (Figure 10) present several anomalies at temperatures: 7.4K, 8.8K, 12.7K and 13.5K. While $T_N = 12.7$K represents the antiferromagnetic ordering temperature, other processes are still unclear. Considering their shapes, they are microscopically different. It would be advantageous to track the phase transitions in field and calculate the respective entropy changes in temperature and field. Further data analysis is to be undergone.

Specific heat for temperatures up to 300K was obtained with a small pulse of 2% using the conventional setup for higher temperatures. Results were fitted with the Einstein model, excluding the low temperature range where phase transitions are observed, as shown in the inset of Figure 10. The obtained Einstein temperature $T_E = (120 \pm 1)$K corresponds to the Debye temperature $T_D = (149 \pm 2)$K, according to the expression [14] $T_D = T_E / \sqrt[3]{\pi/6}$.

Specific heat saturates at $(51 \pm 1)\,\mathrm{JK^{-1}mol^{-1}}$, which is in good agreement with the expected Dulong-Petit value of $50\mathrm{JK^{-1}mol^{-1}}$. A slightly larger value could be ascribed to be a large electronic contribution.

4 Conclusion

A new Al plate setup for the PPMS Heat capacity option provides a way to measure specific heat of magnetically anisotropic materials in large magnetic fields along the hard axis. It produces significant data for investigated RE-Cu compounds in the temperature range where anomalies occur. Above 50K, the sample heat capacity is comparable with the error of the addenda heat capacity and the setup is not applicable. For higher temperature measurements in these materials, the conventional setup must be used.

The measuring and data evaluation procedures were established for RE-Cu materials. Heating pulses of $(10-20)\%$ size are applied to samples attached with Stycast and a post-processing dual-slope method is used for data analysis, performing a moving average of 10% and a 10% exclusion of the initial part of the pulse. Specific heat of ErCu was determined in magnetic fields up to 14T along the $\langle 110 \rangle$ axis.

Additional HoCu, ErCu and TmCu samples with different orientations need to be cut from the existing crystals. Measurements are to be performed along the three significant crystallographic axes. A nonmagnetic equivalent of these RE-Cu compounds, LuCu, will be prepared. Its heat capacity should represent the crystal structure phononic contribution and could be subtracted from the measurements on magnetic RE-Cu to obtain the magnetic contribution.

Other modifications of the setup will ensue. A third design with a platform hanging on Kevlar threads is under construction. It differs from the presented setup inasmuch as the mechanical support, thermal path and electrical wiring, are all decoupled and can be adjusted separately.

References

[1] S. Mühlbauer, B. Binz, F. Jonietz, C. Pfleiderer, B. Rosch, R. Georgii and P. Böni, Skyrmion lattice in a chiral magnet, Science 323 (2009), 915

[2] P. Morin and D. Schmitt, Quadrupolar interactions and magneto-elastic effects in rare eart intermetallic compounds, Ferromagnetic Materials 5 (1990), 5-132

[3] A. Neubauer, C. Pfleiderer, B.Binz, A. Rosch, R. Ritz, PG Niklowitz and P. Böni, Topological Hall effect in the A phase of MnSi, Phys. Rev. Lett. 102 (2009)

[4] P. Morin and D. Schmidt, Competition between multi-q antiferromagnetic structures in cubic rare earth-copper compounds, Journal of Magnetism and Magnetic Materials 21 (1980), 247-258

[5] M. Rahn, Search for topological properties in multi-k magnetic structures, Master thesis (2013), TUM

[6] H. Hautmann, Investigation of the magnetic phase diagram of ErCu, Bachelor thesis (2013), TUM

[7] PPMS User's Manual, Quantum Design (2010)

[8] M. Brando, Development of a relaxation calorimeter for temperatures between 0.05 and 4 K, Rev. Sci. Instrum. (2009)

[9] J. S. Hwang, K. J. Lin and C. Tien, Measurement of heat capacity by fitting the whole temperature response of a heat-pulse calorimeter, Rev. Sci. Instrum. (1997)

[10] J. C. Lashley et al., Critical examination of heat capacity measurements made on a Quantum Design physical property measurement system, Cryogenics 43 (2003), 369-378

[11] R. Bachmann et al., Heat Capacity Measurements on Small Samples at Low Temperatures, Rev. Sci. Insrum. (1972)

[12] A. Bauer, Investigations of itinerant antiferromagnets and cubic chiral helimagnets, PhD thesis (2014), TUM

[13] A dual-slope method for specific heat measurements, J. Phsys. E: Sci. Instrum. 19 790 (1986)

[14] N.W. Ashcroft and N. D. Mermin, Solid State Physics, Saunders, 1976.